

We are IntechOpen, the world's leading publisher of Open Access books Built by scientists, for scientists

6,900

Open access books available

186,000

International authors and editors

200M

Downloads

Our authors are among the

154

Countries delivered to

TOP 1%

most cited scientists

12.2%

Contributors from top 500 universities



WEB OF SCIENCE™

Selection of our books indexed in the Book Citation Index
in Web of Science™ Core Collection (BKCI)

Interested in publishing with us?
Contact book.department@intechopen.com

Numbers displayed above are based on latest data collected.
For more information visit www.intechopen.com



Diversity Management in MIMO-OFDM Systems

Felip Riera-Palou and Guillem Femenias
*Mobile Communications Group
University of the Balearic Islands
Spain*

1. Introduction

Over the last decade, a large degree of consensus has been reached within the research community regarding the physical layer design that should underpin state-of-the-art and future wireless systems (e.g., IEEE 802.11a/g/n, IEEE 802.16e/m, 3GPP-LTE, LTE-Advanced). In particular, it has been found that the combination of multicarrier transmission and multiple-input multiple-output (MIMO) antenna technology leads to systems with high spectral efficiency while remaining very robust against the hostile wireless channel environment.

The vast majority of contemporary wireless systems combat the severe frequency selectivity of the radio channel using orthogonal frequency diversity multiplexing (OFDM) or some of its variants. The theoretical principles of OFDM can be traced back to (Weinstein & Ebert, 1971), however, implementation difficulties delayed the widespread use of this technique well until the late 80s (Cimini Jr., 1985). It is well-known that the combination of OFDM transmission with channel coding and interleaving results in significant improvements from an error rate point of view thanks to the exploitation of the channel frequency diversity (Haykin, 2001, Ch. 6). Further combination with spatial processing using one of the available MIMO techniques gives rise to a powerful architecture, MIMO-OFDM, able to exploit the various diversity degrees of freedom the wireless channel has to offer (Stuber et al., 2004).

1.1 Advanced multicarrier techniques

A significant improvement over conventional OFDM was the introduction of multicarrier code division multiplex (MC-CDM) by Kaiser (2002). In MC-CDM, rather than transmitting a single symbol on each subcarrier, as in conventional OFDM, symbols are code-division multiplexed by means of orthogonal spreading codes and simultaneously transmitted onto the available subcarriers. Since each symbol travels on more than one subcarrier, thus exploiting frequency diversity, MC-CDM offers improved resilience against subcarrier fading. This technique resembles very much the principle behind multicarrier code-division multiple access (MC-CDMA) where each user is assigned a specific spreading code to share a group of subcarriers with other users (Yee et al., 1993).

A more flexible approach to exploit the frequency diversity of the channel is achieved by means of group-orthogonal code-division multiplex (GO-CDM) (Riera-Palou et al., 2008). The idea behind GO-CDM, rooted in a multiple user access scheme proposed in (Cai et al., 2004), is to split suitably interleaved symbols from a given user into orthogonal groups, apply a spreading matrix on a per-subgroup basis and finally map each group to an orthogonal set of

subcarriers. The subcarriers assigned to a group of symbols are typically chosen as separate as possible within the available bandwidth in order to maximise the frequency diversity gain. Note that a GO-CDM setup can be seen as many independent MC-CDM systems of lower dimension operating in parallel. This reduced dimension allows the use of optimum receivers for each group based on maximum likelihood (ML) detection at a reasonable computational cost. In (Riera-Palou et al., 2008), results are given for group dimensioning and spreading code selection. In particular, it is shown that the choice of the group size should take into account the operating channel environment because an exceedingly large group size surely leads to a waste of computational resources, and even to a performance degradation if the channel is not frequency-selective enough. Given the large variation of possible scenarios and equipment configurations in a modern wireless setup, a conservative approach of designing the system to perform satisfactorily in the most demanding type of scenario may lead to a significant waste of computational power, an especially scarce resource in battery operated devices. In fact, large constellation sizes (e.g., 16-QAM, 64-QAM) may difficult the application of GO techniques as the complexity of ML detection can become very high even when using efficient implementations such as the sphere decoder (Fincke & Pohst, 1985). In order to minimise the effects of a mismatch between the operating channel and the GO-CDM architecture, group size adaptation in the context of GO-CDM has been proposed in (Riera-Palou & Femenias, 2009), where it is shown that important complexity reductions can be achieved by dynamically adapting the group size in connection with the sensed frequency diversity of the environment.

1.2 Multiple antennae schemes

Multiple-antenna technology (i.e., MIMO) is the other main enabler towards high speed robust wireless networks. Whereas the use of multiple antennae at the receiver has been long applied as an effective measure to combat fading (see, e.g. (Simon & Alouini, 2005) and references therein), it is the application of multiple antenna at the transmitter side what revolutionised the wireless community. In particular, the linear increase in capacity achieved when jointly increasing the number of antennas at transmission and reception, theoretically forecasted in (Telatar, 1999), has spurred research efforts to effectively realize it in practical schemes. Among these practical schemes, three of them have achieved notable importance in the standardisation of modern wireless communications systems, namely, spatial division multiplexing (SDM), space-time block coding (STBC) and cyclic delay diversity (CDD). While in SDM (Foschini, 1996), independent data streams are sent from the different antennas in order to increase the transmission rate, in STBC (Alamouti, 1998; Tarokh et al., 1999) the multiple transmission elements are used to implement a space-time code targeting the improvement of the error rate performance with respect to that achieved with single-antenna transmission. In CDD (Wittneben, 1993) a single data stream is sent from all transmitter antennae with a different cyclic delay applied to each replica, effectively resulting as if the original stream was transmitted over a channel with increased frequency diversity.

1.3 Chapter objectives

The combination of GO-CDM and MIMO processing, termed MIMO-GO-CDM, results in a powerful and versatile physical layer able to exploit the channel variability in space and frequency. Nevertheless, the different MIMO processing schemes coupled with different degrees of frequency multiplexing (i.e., different group sizes) gives rise to a vast amount of combinations each offering a different operating point in the performance/complexity plane. Choosing an adequate number of Tx/Rx antennas, a specific MIMO scheme and the

subcarrier grouping dimensions can be a daunting task further complicated when Tx and/or Rx antennas are correlated. To this end, it is desirable to have at hand closed-form analytical expressions predicting the performance of the different MIMO-GO-CDM configurations in order to avoid the need of (costly) numerical simulations.

This chapter has two main goals. The first goal is to present a unified BER analysis of the MIMO-GO-CDM architecture. In order to get an insight of the best possible performance this system can offer, attention is restricted to the case when ML detection is employed at the receiver. The analysis is general enough to incorporate the effects of channel frequency selectivity, Tx/Rx antenna correlations and the three most common different forms of spatial processing (SDM, STBC and CDD) in combination with GO-CDM frequential diversity. The analytical results are then used to explore the benefits of GO-CDM under different spatial configurations identifying the most attractive group dimensioning from a performance/complexity perspective. Based on the previous analysis, the second goal of this chapter is to devise effective reconfiguration strategies that can automatically and dynamically fix some of the parameters of the system, more in particular the group size of the GO-CDM component, in response to the instantaneous channel environment with the objective of optimising some pre-defined performance criteria (e.g., error rate, complexity, delay).

The rest of this chapter is organized as follows. Section 2 introduces the system model of a generic MIMO-GO-CDM system, paying special attention to the steps required to implement the frequency spreading and the MIMO processing. In Section 3 a unified BER analysis is presented for the case of ML detection. In light of this analysis, Section 4 explores reconfiguration strategies aiming at the optimisation of several critical parameters of the MIMO-GO-CDM architecture. Numerical results are presented in Section 6 to validate the introduced analytical and reconfiguration procedures. Finally, the main conclusions of this work are recapped in Section 7.

Notational remark: Vectors and matrices are denoted by bold lower and upper case letters, respectively. The superscripts $*$, T and H are used to denote conjugate, transpose and complex transpose (Hermitian), respectively, of the corresponding variable. The operation $vec(\mathbf{A})$ lines up the columns forming matrix \mathbf{A} into a column vector. The symbols \otimes and \odot denote the Kronecker and element-by-element products of two matrices, respectively. Symbols \mathbf{I}_k and $\mathbf{1}_{k \times l}$ denote the k -dimensional identity matrix and an all-ones $k \times l$ matrix, respectively. The symbol $\mathcal{D}(\mathbf{x})$ is used to represent a (block) diagonal matrix having \mathbf{x} at its main (block) diagonal. The determinant of a square matrix \mathbf{A} is represented by $|\mathbf{A}|$ whereas $\|\mathbf{x}\|^2 = \mathbf{x}\mathbf{x}^H$. Expression $\lceil a \rceil$ is used to denote the nearest upper integer of a . Finally, the Alamouti transform of a $K \times 2$ matrix $\mathbf{X} = [\mathbf{x}_1 \ \mathbf{x}_2]$ is defined as $\mathcal{A}(\mathbf{X}) \triangleq [-\mathbf{x}_2^* \ \mathbf{x}_1^*]$.

2. MIMO GO-CDM system model

We consider a MIMO multicarrier system with N_c data subcarriers, equipped with N_T and N_R transmit and receive antennas, respectively, and configured to transmit N_s ($\leq N_T$) spatial data streams. Following the group-orthogonal design principles, the available subcarriers are split into $N_g = N_c/Q$ groups of Q subcarriers each. In the following subsections the transmitter, channel model and reception equation are described in detail.

2.1 Transmitter

As depicted in Fig. 1, incoming bits are split into N_s spatial streams, which are then processed separately. Bits on the z th stream are mapped onto a sequence \mathbf{s}^z of symbols drawn from an

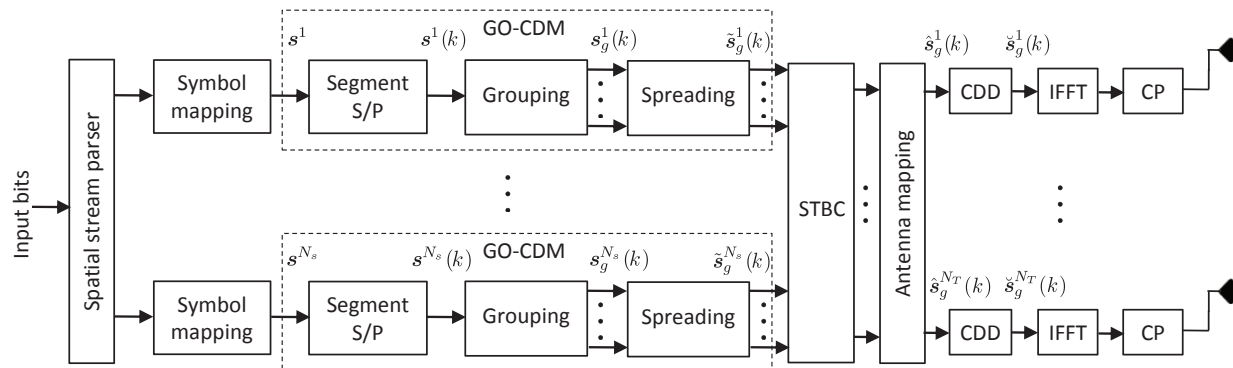


Fig. 1. Transmitter architecture for MIMO GO-CDM.

M -ary complex constellation (e.g. BPSK, M-QAM) with average normalized unit energy. The resulting N_s streams of modulated symbols $\{\mathbf{s}^z\}_{z=1}^{N_s}$ are then fed to the GO-CDM stage, which comprises three steps:

1. Segmentation of the incoming symbol stream in blocks of length N_c (i.e., eventual OFDM symbols), and serial to parallel conversion (S/P) resulting, over the k th OFDM symbol period, in $\mathbf{s}^z(k)$.
2. Arrangement of the symbols in the block into groups $\{\mathbf{s}_g^z(k)\}_{g=1}^{N_g}$, where $\mathbf{s}_g^z(k) = [s_{g,1}^z(k) \dots s_{g,Q}^z(k)]^T$ represents an individual group.
3. Group spreading through a linear combination

$$\tilde{\mathbf{s}}_g^z(k) = \frac{1}{\sqrt{N_T}} \mathbf{C} \mathbf{s}_g^z(k), \quad (1)$$

where \mathbf{C} is a $Q \times Q$ orthonormal matrix, typically chosen to be a rotated Walsh-Hadamard matrix (Riera-Palou et al., 2008).

Before the usual OFDM modulation steps on each antenna (IFFT, guard interval appending and up-conversion), the grouped and spread symbols are processed in accordance with the MIMO transmission scheme in use as follows:

SDM ($N_s = N_T$) : In this case the blocks labeled in Fig. 1 as STBC and CDD are not used, and the spread symbols are directly supplied to the antenna mapping stage, which simply connects the incoming z th data stream to the i th transmit branch ($1 \leq i \leq N_T$), that is,

$$\check{\mathbf{s}}_g^i(k) = \hat{\mathbf{s}}_g^i(k) = \tilde{\mathbf{s}}_g^z(k). \quad (2)$$

STBC ($N_s = 1, N_T = 2$) : Two consecutive blocks of spread symbols, $\tilde{\mathbf{s}}_g^1(k)$ and $\tilde{\mathbf{s}}_g^1(k+1)$, are Alamouti-encoded on a per-subcarrier basis over two OFDM symbol periods,

$$\begin{aligned} \hat{\mathbf{s}}_g^1(k) &= \tilde{\mathbf{s}}_g^1(k), & \hat{\mathbf{s}}_g^1(k+1) &= -\left(\tilde{\mathbf{s}}_g^1(k+1)\right)^*, \\ \hat{\mathbf{s}}_g^2(k) &= \tilde{\mathbf{s}}_g^1(k+1), & \hat{\mathbf{s}}_g^2(k+1) &= \left(\tilde{\mathbf{s}}_g^1(k)\right)^*. \end{aligned} \quad (3)$$

In the antenna mapping stage, STBC-encoded streams are connected to two transmit branches, one for each symbol of the STBC code, that is,

$$\check{s}_g^i(k) = \hat{s}_g^i(k). \quad (4)$$

CDD ($N_s = 1$) : In a pure CDD scheme, the same data stream is sent through N_T antennas with each replica being subject to a different cyclic delay Δ_i , typically chosen as $\Delta_i = \Delta_{i-1} + N_c/N_T$ with $\Delta_1 = 0$ (Bauch & Malik, 2006), resulting in transmitted symbols

$$\check{s}_{g,q}^i(k) = \hat{s}_{g,q}^1(k) \exp(-j2\pi d_q \Delta_i / N_c), \quad (5)$$

where d_q denotes the subcarrier index.

Hybrid schemes The analytical framework developed in this chapter can also be applied to hybrid systems combining SDM, STBC and/or CDD. Nevertheless, for brevity of presentation, the analysis to be developed next focuses on scenarios where only one of the mechanisms is used.

2.2 Channel model

The channel linking an arbitrary pair of Tx and Rx antennas is assumed to be time-varying and frequency-selective with an scenario-dependent power delay profile

$$S(\tau) = \sum_{l=0}^{P-1} \phi_l \delta(\tau - \tau_l), \quad (6)$$

where P denotes the number of independent paths of the channel and ϕ_l and τ_l denote the power and delay of the l -th path. It is assumed that the power delay profile is the same for all pairs of Tx and Rx antennas and that it has been normalized to unity (i.e., $\sum_{l=0}^{P-1} \phi_l = 1$). A single realization of the channel impulse response between Tx antenna i and receive antenna j at time instant t will then have the form

$$h^{ij}(t; \tau) = \sum_{l=0}^{P-1} h_l^{ij}(t) \delta(\tau - \tau_l), \quad (7)$$

where it will hold that $E \{ |h_l^{ij}(t)|^2 \} = \phi_l$. The corresponding frequency response can be expressed as

$$\bar{h}^{ij}(t; f) = \sum_{l=0}^{P-1} h_l^{ij}(t) \exp(-j2\pi f \tau_l), \quad (8)$$

which when evaluated at the N_c OFDM subcarriers yields

$$\bar{\mathbf{h}}^{ij}(t) = [\bar{h}^{ij}(t; f_0) \dots \bar{h}^{ij}(t; f_{N_c-1})]^T. \quad (9)$$

In order to simplify the notation, assuming that the channel is static over the duration of a block (i.e., an OFDM symbol), the frequency response between Tx-antenna i and Rx-antenna j over the N_c subcarriers during the k th OFDM symbol can be expressed as

$$\bar{\mathbf{h}}^{ij}(k) = [\bar{h}_0^{ij}(k) \dots \bar{h}_{N_c-1}^{ij}(k)]^T. \quad (10)$$

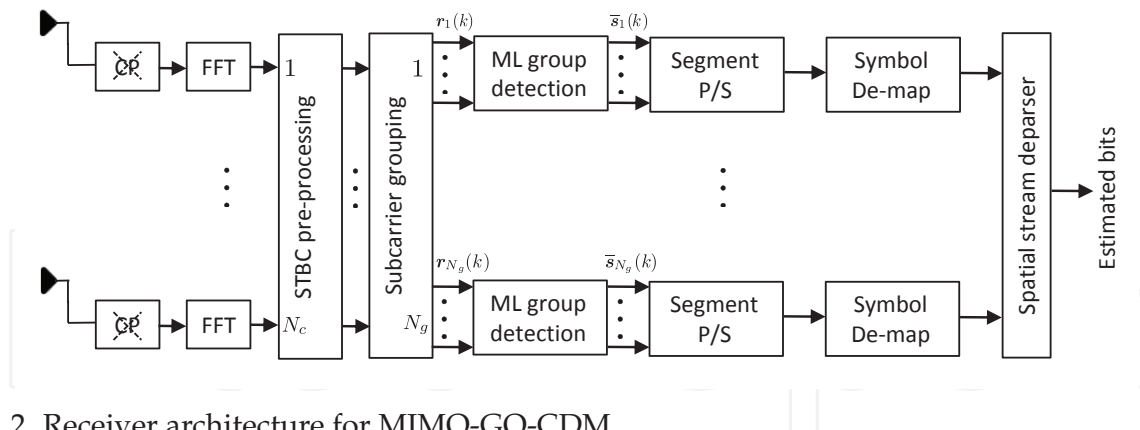


Fig. 2. Receiver architecture for MIMO-GO-CDM.

Since the subsequent analysis is mostly conducted on per-group basis, the channel frequency response for the g th group is denoted by

$$\bar{\mathbf{h}}_g^{ij}(k) = [\bar{h}_{g,1}^{ij}(k) \dots \bar{h}_{g,Q}^{ij}(k)]^T, \quad (11)$$

with correlation matrix given by

$$\mathcal{R}_{h_g} = E \left\{ \|\bar{\mathbf{h}}_g^{ij}(k)\|^2 \right\} = E \left\{ \bar{\mathbf{h}}_g^{ij}(k) \left(\bar{\mathbf{h}}_g^{ij}(k) \right)^H \right\}, \quad (12)$$

which is assumed to be constant over time, common for all pairs of Tx and Rx antennas and, provided that group subcarriers are chosen equispaced across the available bandwidth, common to all groups.

Now, considering the spatial correlation introduced by the transmit and receive antenna arrays, the spatially correlated channel frequency response for an arbitrary subcarrier q in group g can be expressed as (van Zelst & Hammerschmidt, 2002)

$$\mathcal{H}_{g,q}(k) = \mathcal{R}_{RX}^{1/2} \mathbf{H}_{g,q}(k) \left(\mathcal{R}_{TX}^{1/2} \right)^T, \quad (13)$$

where \mathcal{R}_{RX} and \mathcal{R}_{TX} are, respectively, $N_R \times N_R$ and $N_T \times N_T$ matrices denoting the receive and transmit correlation, and

$$\mathbf{H}_{g,q}(k) = \begin{pmatrix} \bar{h}_{g,q}^{11}(k) & \dots & \bar{h}_{g,q}^{1N_T}(k) \\ \vdots & & \vdots \\ \bar{h}_{g,q}^{N_R 1}(k) & \dots & \bar{h}_{g,q}^{N_R N_T}(k) \end{pmatrix}. \quad (14)$$

2.3 Receiver

As shown in Fig. 2, the reception process begins by removing the cyclic prefix and performing an FFT to recover the symbols in the frequency domain. After S/P conversion, and assuming ideal synchronization at the receiver side, the received samples for group g at the output of the FFT processing stage can be expressed in accordance with the MIMO transmission scheme in use as follows:

SDM and CDD: In these cases,

$$\mathbf{r}_g(k) = \text{vec} \left(\left[\mathbf{r}_{g,1}(k) \dots \mathbf{r}_{g,Q}(k) \right] \right) = \mathbf{H}_g(k) \check{\mathbf{s}}_g(k) + \mathbf{v}_g(k), \quad (15)$$

where the $N_R Q \times N_T Q$ matrix

$$\mathbf{H}_g(k) = \mathcal{D} \left(\left[\mathbf{H}_{g,1}(k) \dots \mathbf{H}_{g,Q}(k) \right] \right), \quad (16)$$

represents the spatially and frequency correlated channel matrix affecting all symbols transmitted in group g , the $N_s Q$ -long vector of transmitted (spread) symbols is formed as

$$\check{\mathbf{s}}_g(k) = \text{vec} \left(\left[\check{\mathbf{s}}_g^1(k) \dots \check{\mathbf{s}}_g^{N_T}(k) \right]^T \right), \quad (17)$$

and finally, $\mathbf{v}_g(k)$ is an $N_R Q \times 1$ vector representing the receiver noise, with each component being drawn from a circularly symmetric zero-mean white Gaussian distribution with variance σ_v^2 .

STBC: As stated in (3), STBC encoding period $\eta = k/2$, with $k = 0, 2, 4, \dots$, spawns two consecutive OFDM symbol periods, namely, the k th and $(k+1)$ th symbol periods. Assuming that the channel coherence time is large enough to safely consider that $\mathbf{H}_g(k+1) = \mathbf{H}_g(k)$, then,

$$\begin{aligned} \tilde{\mathbf{r}}_g(k) &= \mathbf{H}_g(k) \check{\mathbf{s}}_g(k) + \mathbf{v}_g(k), \\ \tilde{\mathbf{r}}_g(k+1) &= \mathbf{H}_g(k) \check{\mathbf{s}}_g(k+1) + \mathbf{v}_g(k+1), \end{aligned} \quad (18)$$

and, therefore, we can define an equivalent received vector in STBC encoding period η as

$$\mathbf{r}_g(\eta) \triangleq \begin{bmatrix} \tilde{\mathbf{r}}_g(k) \\ \tilde{\mathbf{r}}_g^*(k+1) \end{bmatrix} = \begin{bmatrix} \mathbf{H}_g(k) \\ \mathbf{H}_g^A(k) \end{bmatrix} \check{\mathbf{s}}_g(\eta) + \begin{bmatrix} \mathbf{v}_g(k) \\ \mathbf{v}_g^*(k+1) \end{bmatrix} \triangleq \tilde{\mathbf{H}}_g(\eta) \check{\mathbf{s}}_g(\eta) + \tilde{\mathbf{v}}_g(\eta), \quad (19)$$

where

$$\mathbf{H}_g^A(k) \triangleq \mathcal{D} \left(\left[\mathcal{A}(\mathbf{H}_{g,1}(k)) \dots \mathcal{A}(\mathbf{H}_{g,Q}(k)) \right] \right) \quad (20)$$

and

$$\check{\mathbf{s}}_g(\eta) \triangleq \text{vec} \left(\left[\check{\mathbf{s}}_g^1(k) \check{\mathbf{s}}_g^1(k+1) \right]^T \right). \quad (21)$$

In order to facilitate the unified performance analysis of the different MIMO strategies, it is more convenient to express the reception equation in terms of the original symbols rather than the spread ones. Thus, defining

$$\begin{aligned} \mathbf{s}_g(k) &= \frac{1}{\sqrt{N_T}} \text{vec} \left(\left[\mathbf{s}_g^1(k) \dots \mathbf{s}_g^{N_s}(k) \right]^T \right) && \text{SDM} \\ \mathbf{s}_g(\eta) &= \frac{1}{\sqrt{2}} \text{vec} \left(\left[\mathbf{s}_g^1(k) \mathbf{s}_g^1(k+1) \right]^T \right) && \text{STBC} \\ \mathbf{s}_g(k) &= \frac{1}{\sqrt{N_T}} \mathbf{s}_g^1(k) && \text{CDD} \end{aligned} \quad (22)$$

it is straightforward to check that the symbols to be supplied to the IFFT processing step are given by,

$$\begin{aligned} \check{\mathbf{s}}_g(k) &= (\mathbf{C} \otimes \mathbf{I}_{N_s}) \mathbf{s}_g(k) && \text{SDM} \\ \check{\mathbf{s}}_g(k) &= \check{\mathbf{s}}_g(\eta) = (\mathbf{C} \otimes \mathbf{I}_2) \mathbf{s}_g(\eta) && \text{STBC} \\ \check{\mathbf{s}}_g(k) &= \mathbf{E}_g^A (\mathbf{C} \otimes \mathbf{1}_{N_T \times 1}) \mathbf{s}_g(k) && \text{CDD} \end{aligned}$$

with $\mathbf{E}_g^\Delta \triangleq \mathcal{D} \left(\left[\mathbf{E}_g^{\Delta 1} \dots \mathbf{E}_g^{\Delta Q} \right] \right)$, where $\mathbf{E}_g^{\Delta q} = \mathcal{D} \left(\left[e^{-j2\pi d_q \Delta_1 / N_c} \dots e^{-j2\pi d_q \Delta_{N_T} / N_c} \right] \right)$ (Bauch & Malik, 2006). Furthermore, since processing takes place either on an OFDM symbol basis for SDM and CDD systems or on an STBC encoding period basis for STBC schemes, the indexes k and/or η can be dropped from this point onwards, allowing the reception equation to be expressed in general form as

$$\mathbf{r}_g = \mathbf{A}_g \mathbf{s}_g + \boldsymbol{\nu}_g$$

where

$$\mathbf{A}_g = \begin{cases} \mathcal{H}_g (\mathbf{C} \otimes \mathbf{I}_{N_s}) & \text{SDM} \\ \tilde{\mathcal{H}}_g (\mathbf{C} \otimes \mathbf{I}_2) & \text{STBC} \\ \mathcal{H}_g \mathbf{E}_g^\Delta (\mathbf{C} \otimes \mathbf{1}_{N_T \times 1}) & \text{CDD} \end{cases}$$

and

$$\boldsymbol{\nu}_g = \begin{cases} \mathbf{v}_g & \text{for SDM/CDD} \\ \tilde{\mathbf{v}}_g & \text{for STBC} \end{cases} . \quad (23)$$

It should be noted that, regardless of the MIMO scheme and group dimension in use, the system matrix \mathbf{A}_g has been normalised such that the SNR can be defined as $E_s / N_0 = 1 / (2\sigma_v^2)$. Upon reception, all symbols in a group (for all streams in SDM and for both encoded OFDM symbols in STBC) are jointly estimated using an ML detection process. That is, the vector of estimated symbols in a group can be expressed as

$$\bar{\mathbf{s}}_g = \arg \min_{\mathbf{s}_g} \|\mathbf{A}_g \mathbf{s}_g - \mathbf{r}_g\|^2. \quad (24)$$

This procedure amounts to evaluate all the possible transmitted vectors and choosing the closest one (in a least-squares sense) to the received vector. Nevertheless, sphere detection (Fincke & Pohst, 1985) can be used for efficiently performing the exhaustive search required to implement the ML estimation.

3. Unified bit error rate analysis

3.1 BER analysis based on pairwise error probability

Using the well-known union bound (Simon et al., 1995), which is very tight for high signal-to-noise ratios, the bit error probability can be upper bounded as

$$P_b \leq \frac{1}{N_g N_Q M^{N_Q} \log_2 M} \sum_{g=1}^{N_g} \sum_{u=1}^{M^{N_Q}} \sum_{\substack{w=1 \\ w \neq u}}^{M^{N_Q}} P(\mathbf{s}_{g,u} \rightarrow \mathbf{s}_{g,w}) \mathcal{N}_b(\mathbf{s}_{g,u}, \mathbf{s}_{g,w}), \quad (25)$$

where,

$$N_Q = \begin{cases} Q N_s & \text{for SDM} \\ 2Q & \text{for STBC} \\ Q & \text{for CDD} \end{cases} . \quad (26)$$

The expression $P(\mathbf{s}_{g,u} \rightarrow \mathbf{s}_{g,w})$, usually called the pairwise error probability (PEP), represents the probability of erroneously detecting the vector $\mathbf{s}_{g,w}$ when $\mathbf{s}_{g,u}$ was transmitted and

$\mathcal{N}_b(\mathbf{s}_{g,u}, \mathbf{s}_{g,w})$ is equal to the number of differing bits between vectors $\mathbf{s}_{g,u}$ and $\mathbf{s}_{g,w}$. To proceed further, the PEP conditioned on \mathbf{A}_g can be shown to be (Craig, 1991)

$$\begin{aligned}
 P(\mathbf{s}_{g,u} \rightarrow \mathbf{s}_{g,w} | \mathbf{A}_g) &= \frac{1}{2} \operatorname{erfc} \left(\sqrt{\frac{\|\mathbf{A}_g(\mathbf{s}_{g,u} - \mathbf{s}_{g,w})\|^2}{4\sigma_v^2}} \right) \\
 &= \frac{1}{\pi} \int_0^{\pi/2} \exp \left(-\frac{\|\mathbf{A}_g(\mathbf{s}_{g,u} - \mathbf{s}_{g,w})\|^2}{4\sigma_v^2 \sin^2 \phi} \right) d\phi.
 \end{aligned}
 \tag{27}$$

Now, defining the random variable $d_{g,uw}^2 \triangleq \|\mathbf{A}_g(\mathbf{s}_{g,u} - \mathbf{s}_{g,w})\|^2$, the unconditional PEP can be expressed as

$$\begin{aligned}
 P(\mathbf{s}_{g,u} \rightarrow \mathbf{s}_{g,w}) &= \frac{1}{\pi} \int_0^{\pi/2} \int_{-\infty}^{+\infty} e^{-x/4\sigma_v^2 \sin^2 \phi} p_{d_{g,uw}^2}(x) dx d\phi \\
 &= \frac{1}{\pi} \int_0^{\pi/2} \mathcal{M}_{d_{g,uw}^2} \left(-\frac{1}{4\sigma_v^2 \sin^2 \phi} \right) d\phi,
 \end{aligned}
 \tag{28}$$

where $p_x(\cdot)$ and $\mathcal{M}_x(\cdot)$ denote the probability density function (pdf) and moment generating function (MGF) of a random variable x , respectively.

Let us now define the error vector $\mathbf{e}_{g,uw} = \mathbf{s}_{g,u} - \mathbf{s}_{g,w}$. Using this definition, it can be shown that

$$d_{g,uw}^2 \triangleq \|\mathbf{A}_g \mathbf{e}_{g,uw}\|^2 = \mathbf{H}_g^H \mathbf{T}_{g,uw}^H \mathbf{T}_{g,uw} \mathbf{H}_g,
 \tag{29}$$

where

$$\mathbf{H}_g \triangleq \operatorname{vec} \left[\operatorname{vec}(\mathbf{H}_{g,1}) \dots \operatorname{vec}(\mathbf{H}_{g,Q}) \right],
 \tag{30}$$

and $\mathbf{T}_{g,uw}$ can be expressed as

$$\mathbf{T}_{g,uw} = \begin{cases} \left[\left(\mathbf{1}_{Q \times 1} \otimes \mathbf{S}_{g,uw} \right) \odot \mathfrak{I}_{Q,N_T} \right] \otimes \mathbf{I}_{N_R} & \text{SDM/CDD} \\ \left[\left(\mathbf{1}_{1 \times Q} \otimes \mathbf{S}_{g,uw}^T \right) \odot \mathfrak{I}_{Q,2}^T \right] \otimes \mathbf{I}_{2N_R} & \text{STBC} \end{cases}
 \tag{31}$$

with

$$\mathbf{S}_{g,uw} = \begin{cases} \mathbf{e}_{g,uw}^T (\mathbf{C}^T \otimes \mathbf{I}_{N_T}) & \text{SDM/STBC} \\ \mathbf{e}_{g,uw}^T (\mathbf{C}^T \otimes \mathbf{1}_{1 \times N_T}) \mathbf{E}_\Delta^T & \text{CDD} \end{cases}
 \tag{32}$$

and $\mathfrak{I}_{n,m} \triangleq \mathbf{I}_n \otimes \mathbf{1}_{1 \times m}$. The expression of $d_{g,uw}^2$ reveals that it is a quadratic form in complex variables \mathbf{H}_g , with MGF given by

$$\mathcal{M}_{d_{g,uw}^2}(s) = |\mathbf{I}_N - s\mathbf{G}_{g,uw}|^{-1},
 \tag{33}$$

where N is equal to QN_R for the SDM and CDD schemes, and equal to $4QN_R$ for the STBC strategy. Furthermore,

$$\mathbf{G}_{g,uw} = \mathbf{T}_{g,uw} \mathbf{R}_g \mathbf{T}_{g,uw}^H,
 \tag{34}$$

with

$$\mathbf{R}_g = \mathbf{R}_{h_g} \otimes \mathbf{R}_{TX} \otimes \mathbf{R}_{RX}.
 \tag{35}$$

Now, let $\lambda_{g,uw} = \{\lambda_{g,uw,1}, \dots, \lambda_{g,uw,D_{g,uw}}\}$ denote the set of $D_{g,uw}$ distinct positive eigenvalues of $\mathbf{G}_{g,uw}$ with corresponding multiplicities $\alpha_{g,uw} = \{\alpha_{g,uw,1}, \dots, \alpha_{g,uw,D_{g,uw}}\}$. Using the results in (Femenias, 2004), the MGF of $d_{g,uw}^2$ can also be expressed as

$$\mathcal{M}_{d_{g,uw}^2}(s) = \prod_{d=1}^{D_{g,uw}} \frac{1}{(1 - s\lambda_{g,uw,d})^{\alpha_{g,uw,d}}} = \sum_{d=1}^{D_{g,uw}} \sum_{p=1}^{\alpha_{g,uw,d}} \frac{\kappa_{g,uw,d,p}}{(1 - s\lambda_{g,uw,d})^p} \quad (36)$$

where, using (Amari & Misra, 1997, Theorem 1), it can be shown that

$$\begin{aligned} \kappa_{g,uw,d,p} &= \frac{\lambda_{g,uw,d}^{p-\alpha_{g,uw,d}}}{(\alpha_{g,uw,d} - p)!} \frac{\partial^{\alpha_{g,uw,d}-p}}{\partial s^{\alpha_{g,uw,d}-p}} \left[\prod_{\substack{d'=1 \\ d' \neq d}}^{D_{g,uw}} \frac{1}{(1 - s\lambda_{g,uw,d'})^{\alpha_{g,uw,d'}}} \right] \Bigg|_{s=\frac{1}{\lambda_{g,uw,d}}} \\ &= \lambda_{g,uw,d}^{p-\alpha_{g,uw,d}} \sum_{\Phi} \prod_{\substack{d'=1 \\ d' \neq d}}^{D_{g,uw}} \frac{\lambda_{g,uw,d'}^{n_{d'}} \binom{\alpha_{g,uw,d'} + n_{d'} - 1}{n_{d'}}}{\left(1 - \frac{\lambda_{g,uw,d'}}{\lambda_{g,uw,d}}\right)^{\alpha_{g,uw,d'} + n_{d'}}} \end{aligned} \quad (37)$$

with Φ being the set of nonnegative integers $\{n_1, \dots, n_{d-1}, n_{d+1}, \dots, n_{D_{g,uw}}\}$ such that $\sum_{d' \neq d} n_{d'} = \alpha_{g,uw,d} - p$, which allows (28) to be written as

$$\begin{aligned} P(\mathbf{s}_{g,u} \rightarrow \mathbf{s}_{g,w}) &= \frac{1}{\pi} \sum_{d=1}^{D_{g,uw}} \sum_{p=1}^{\alpha_{g,uw,d}} \kappa_{g,uw,d,p} \int_0^{\pi/2} \left(\frac{\sin^2 \phi}{\sin^2 \phi + \frac{\lambda_{g,uw,d}}{4\sigma_v^2}} \right)^p d\phi \\ &= \sum_{d=1}^{D_{g,uw}} \sum_{p=1}^{\alpha_{g,uw,d}} \kappa_{g,uw,d,p} \left(\frac{1 - \Omega\left(\frac{\lambda_{g,uw,d}}{4\sigma_v^2}\right)}{2} \right)^p \sum_{g=0}^{p-1} \binom{p-1+g}{g} \left(\frac{1 + \Omega\left(\frac{\lambda_{g,uw,d}}{4\sigma_v^2}\right)}{2} \right)^g, \end{aligned} \quad (38)$$

with $\Omega(c) = \sqrt{c/(1+c)}$. By substituting (38) into (25), a closed-form BER upper bound for an arbitrary power delay profile is obtained. It is later shown that this bound is tight, accurately matching the simulation results.

3.2 BER analysis based on PEP classes

Since there are many pairs $(\mathbf{s}_{g,u}, \mathbf{s}_{g,w})$ giving exactly the same PEP, it is possible to define a pairwise error class $\mathcal{C}(D_{g,c}, \lambda_{g,c}, \alpha_{g,c})$ as the set of all pairs $(\mathbf{s}_{g,u}, \mathbf{s}_{g,w})$ characterized by a common matrix $\mathbf{G}_{g,uw} = \mathbf{G}_{g,c}$ with $D_{g,c}$ distinct eigenvalues $\lambda_{g,c} = \{\lambda_{g,c,1}, \dots, \lambda_{g,c,D_{g,c}}\}$ with corresponding multiplicities $\alpha_{g,c} = \{\alpha_{g,c,1}, \dots, \alpha_{g,c,D_{g,c}}\}$ and therefore, a common PEP denoted by $\mathcal{P}(D_{g,c}, \lambda_{g,c}, \alpha_{g,c})$. A more insightful BER expression can then be obtained by using the PEP class notation, avoiding in this way the exhaustive computation of all the PEPs. Instead, the BER upper-bound can be found by computing the PEP for each class and weighing it using the number of elements in the class and the number of erroneous bits this class may induce. The BER upper bound can then be rewritten as

$$\begin{aligned} P_b &\leq \frac{1}{N_g N_Q M^{N_Q} \log_2 M} \\ &\quad \times \sum_{g=1}^{N_g} \sum_{\forall \mathcal{C}(D_{g,c}, \lambda_{g,c}, \alpha_{g,c})} \sum_{\mathcal{N}=1}^{N_Q \log_2 M} \mathcal{N} W(D_{g,c}, \lambda_{g,c}, \alpha_{g,c}, \mathcal{N}) \mathcal{P}(D_{g,c}, \lambda_{g,c}, \alpha_{g,c}), \end{aligned} \quad (39)$$

where $W(D_{g,c}, \lambda_{g,c}, \alpha_{g,c}, \mathcal{N})$ corresponds to the number of elements in the class $\mathcal{C}(D_{g,c}, \lambda_{g,c}, \alpha_{g,c})$ inducing \mathcal{N} erroneous bits.

3.3 Asymptotic performance

Now, in order to gain further insight on the parameters affecting the BER performance, let us focus on the asymptotic case of large SNR. When $E_s/N_0 \rightarrow \infty$, the argument of the MGF in (28) also tends to infinity, and it can easily be shown that when $s \rightarrow \infty$ the MGF in (36) can be approximated by

$$\mathcal{M}_{d_{g,uv}^2}(s) \simeq \frac{1}{\left(\prod_{d=1}^{D_{g,uv}} \lambda_{g,uv,d}^{\alpha_{g,uv,d}}\right) (-s)^{\sum_{d=1}^{D_{g,uv}} \alpha_{g,uv,d}}}, \tag{40}$$

allowing the asymptotic PEP of the different classes to be expressed as

$$\mathcal{P}_{\text{asym}}(D_{g,c}, \lambda_{g,c}, \alpha_{g,c}) = \frac{1}{\pi} \int_0^{\pi/2} \frac{(4\sigma_v^2 \sin^2 \phi)^{\tilde{D}_{g,c}}}{\prod_{d=1}^{D_{g,c}} \lambda_{g,c,d}^{\alpha_{g,c,d}}} d\phi = \frac{(2\tilde{D}_{g,c})! (E_s/N_0)^{-\tilde{D}_{g,c}}}{2\tilde{D}_{g,c}!^2 \prod_{d=1}^{\tilde{D}_{g,c}} \lambda_{g,c,d}^{\alpha_{g,c,d}}}, \tag{41}$$

where $\tilde{D}_{g,c} = \sum_{d=1}^{D_{g,c}} \alpha_{g,c,d}$ is the rank of the matrix-defining class $\mathbf{G}_{g,c}$. From (41) it is clear that the probability of error will be mainly determined by the groups and classes whose matrices

$$\mathbf{G}_{g,c} = \mathbf{G}_{g,c}^{\min} \triangleq \mathbf{T}_{g,c}^{\min} \mathbf{R}_g^{\min} \left(\mathbf{T}_{g,c}^{\min}\right)^H \tag{42}$$

have the smallest common rank, denoted by

$$\tilde{D}_{\min} = \text{rank}(\mathbf{G}_{g,c}^{\min}) = \text{rank} \left(\mathbf{T}_{g,c}^{\min} \mathbf{R}_g^{\min} \left(\mathbf{T}_{g,c}^{\min}\right)^H\right), \tag{43}$$

allowing the asymptotic BER to be written as

$$P_b \leq \sum_{g=1}^{N_g} \sum_{\forall \mathcal{C}(\tilde{D}_{\min}, \lambda_{g,c}, \alpha_{g,c})} \sum_{\mathcal{N}=1}^{N_Q \log_2 M} \mathcal{N} \frac{(2\tilde{D}_{\min})!}{2(\tilde{D}_{\min}!)^2} \frac{W(\tilde{D}_{\min}, \lambda_{g,c}, \alpha_{g,c}, \mathcal{N}) (E_s/N_0)^{-\tilde{D}_{\min}}}{N_g N_Q M^{N_Q} \log_2 M \prod_{d=1}^{\tilde{D}_{\min}} \lambda_{g,c,d}^{\alpha_{g,c,d}}}. \tag{44}$$

In light of (44), the asymptotic BER minimisation is achieved by maximising the minimum group/class rank \tilde{D}_{\min} and the eigenvalue product of all the groups/classes with rank \tilde{D}_{\min} . In the following, only the maximization of \tilde{D}_{\min} (i.e., maximisation of the diversity order) is pursued since the maximization of the product of eigenvalues is far more difficult as it involves the simultaneous optimization of all the eigenvalue products in the groups/classes with rank \tilde{D}_{\min} .

On the rank of $\mathbf{T}_{g,c}^{\min}$: As stated in (Cai et al., 2004; Riera-Palou et al., 2008), choosing the subcarriers for a group equispaced across the whole bandwidth minimizes subcarrier correlation allowing the optimization of the system performance if an adequate family of spreading codes is properly selected. To this end, rotated spreading transforms have been proposed for multicarrier systems in (Bury et al., 2003) where it is shown that the often used Walsh-Hadamard codes lead to poor diversity gains when employed to perform the frequency spreading. This can be explained by the fact that for certain symbol blocks the energy is concentrated on one single subcarrier and, thus,

$$\text{rank} \left(\mathbf{T}_{g,c}^{\min}\right) = \begin{cases} N_R & \text{SDM} \\ N_T N_R & \text{STBC/CDD.} \end{cases} \tag{45}$$

A deep fade on this subcarrier dramatically raises the probability of error in the detection process, regardless of the state of all other subcarriers, limiting in this way the achievable diversity order (asymptotic BER slope). A similar effect can be observed when using other spreading sequences such as those based on the discrete Fourier transform (DFT). As pointed out in (Bury et al., 2003), a spreading that has the potential to maximize the diversity order can be found by applying a rotation to the columns of the conventional spreading matrix \mathbf{C}_{conv} as $\mathbf{C} = \mathbf{C}_{\text{conv}}\mathcal{D}(\boldsymbol{\theta})$, where $\boldsymbol{\theta} = [\theta_1 \dots \theta_Q]$ with each θ_q denoting the chip-specific rotation, which in the proposed scheme is given by

$$\theta_q = \exp\left(\frac{j2\pi(q-1)}{Q\Theta}\right),$$

with Θ being constellation dependent and selected so as to make $2\pi/\Theta$ the minimum angle producing a rotation of the transmit symbol alphabet onto itself (e.g., $\Theta = 2$ for BPSK, $\Theta = 4$ for MQAM). This indicates that while using conventional Walsh-Hadamard spreading no frequency diversity gain will be achieved, the rotated spreading has the potential (depending on the channel correlation matrix \mathbf{R}_g) to attain a frequency diversity gain proportional to the number of subcarriers per group, common to all groups and classes. That is, when using optimally rotated spreading codes,

$$\text{rank}\left(\mathbf{T}_{g,c}^{\min}\right) = \begin{cases} Q N_R & \text{SDM} \\ Q N_T N_R & \text{STBC/CDD.} \end{cases} \quad (46)$$

On the rank of \mathbf{R}_g^{\min} : The correlation matrix \mathbf{R}_g^{\min} can be expressed in general form as

$$\mathbf{R}_g^{\min} = \mathcal{R}_{h_g}^{\min} \otimes \mathcal{R}_{TX} \otimes \mathcal{R}_{RX}, \quad (47)$$

and consequently (Petersen & Pedersen, 2008),

$$\text{rank}\left(\mathbf{R}_g^{\min}\right) = \text{rank}\left(\mathcal{R}_{h_g}^{\min}\right) \text{rank}\left(\mathcal{R}_{TX}\right) \text{rank}\left(\mathcal{R}_{RX}\right). \quad (48)$$

Except for pathological setups exhibiting full spatial correlation between pairs of transmit or receive antennas (scenario not considered in this analysis), \mathcal{R}_{TX} and \mathcal{R}_{RX} are full rank matrices with $\text{rank}\left(\mathcal{R}_{TX}\right) = N_T$ and $\text{rank}\left(\mathcal{R}_{RX}\right) = N_R$, and therefore,

$$\text{rank}\left(\mathbf{R}_g^{\min}\right) = N_T N_R \text{rank}\left(\mathcal{R}_{h_g}^{\min}\right). \quad (49)$$

Therefore, the maximum attainable frequency diversity order can be directly related to $\mathcal{R}_{h_g}^{\min}$ and is given by the number of independent paths in the channel delay profile. If error performance is to be optimized, enough subcarriers per group need to be allocated to ensure that $\text{rank}\left(\mathcal{R}_{h_g}^{\min}\right) = P$. In fact, defining the sampled channel order L as the channel delay spread in terms of chip (sampling) periods, it is shown in Cai et al. (2004) that the maximum rank of $\mathcal{R}_{h_g}^{\min}$ is attained by setting the number of subcarriers per group to $Q = L + 1$. While this is a valuable design rule in channels with short delay spread, in most practical scenarios where L can be in the order of tens or even hundreds of samples, the theoretical number of subcarriers required to achieve full diversity would make the use of ML detection difficult even when using efficient search strategies (i.e., sphere decoding).

Moreover, very often maximum diversity would only be attained at unreasonably large E_s/N_0 levels.

In order to determine the number of subcarriers worth using in a given environment (i.e., a particular channel power delay profile), it is useful to use as reference the characteristics of the ideal case where all subcarriers in the group are fully uncorrelated (frequency domain *iid* channel). It is straightforward to see that, in this case, the frequency correlation matrix is given by $\mathcal{R}_{h_g}^{\min} = \mathbf{I}_Q$, with $\text{rank}(\mathcal{R}_{h_g}^{\min}) = Q$, and furthermore, it has only one non-zero eigenvalue $\lambda_{h_g,1} = 1$ with multiplicity $\alpha_{h_g,1} = Q$. Therefore, for any given MIMO configuration and a fixed number of subcarriers, the frequency domain *iid* channel results in the maximum frequency diversity order (Q) and will also lead to the minimum probability of error.

Since, for most realistic scenarios, setting the group size to guarantee full diversity ($Q = L + 1$) is unfeasible, we need to be able to measure what each additional subcarrier is contributing in terms of frequency diversity gain. Ideally, each additional subcarrier should bring along an extra diversity order, that is, an increase in $\text{rank}(\mathcal{R}_{h_g}^{\min})$ by one as it is indeed the case for uncorrelated channels. For correlated channels, however, this is often not the case and therefore to choose the group size it is useful to have some form of measure. A widely used tool in principal component analysis (Johnson & Wichern, 2002) to assess the *practical* dimensionality of a correlation matrix is the cumulative sum of eigenvalues (CSE) that, for the correlation matrix $\mathcal{R}_{h_g}^{\min}$ with eigenvalues $\{\lambda_{h_g,q}\}_{q=1}^Q$, is defined as

$$\Psi(n) = \frac{\sum_{q=1}^n \lambda_{h_g,q}}{\sum_{q=1}^Q \lambda_{h_g,q}}. \quad (50)$$

For the frequency domain *iid* channel, $\Psi(n)$ is always a discrete linearly increasing function of n , and it can serve as a reference against which to measure the contribution of each subcarrier in arbitrary realistic channels.

As an example, suppose we are trying to determine the appropriate group size for models B and E from the propagation studies conducted in the definition of IEEE 802.11n (Erceg, 2003). Both models have been measured across a total bandwidth of 20 MHz with a channel sampling chip period of 10 ns. On one hand Model B is made of 11 paths and it has an *rms*-delay spread of 15 ns and very low frequency selectivity. On the other hand Model E corresponds to a channel with 38 paths (split in 4 clusters) with an *rms*-delay spread of 100 ns, resulting in large frequency selectivity. While Model B is representative of typical office indoor environments, Model E corresponds to large outdoor spaces such as airports or sport halls.

Figure 3 depicts the CSE for channel profiles B, E and the *iid* model, for different number of subcarriers ($Q = 2, 4, 8$ or 16) chosen equispaced across a bandwidth of 20 MHz. It can be inferred from the top left plot that when only two subcarriers are used per group ($Q = 2$), Models B and E behave qualitatively in a similar manner to the *iid* model and each of the subcarriers contributes in a significant way towards the achievement of the maximum diversity. When increasing the number of subcarriers (e.g., $Q = 4, 8, 16$), this no longer holds, notice how the CSE values for Model B quickly saturate and get farther apart from those of the *iid* channel, indicating that the additional subcarriers do not contribute substantially in increasing the frequency diversity order. For the case of Model E, a similar

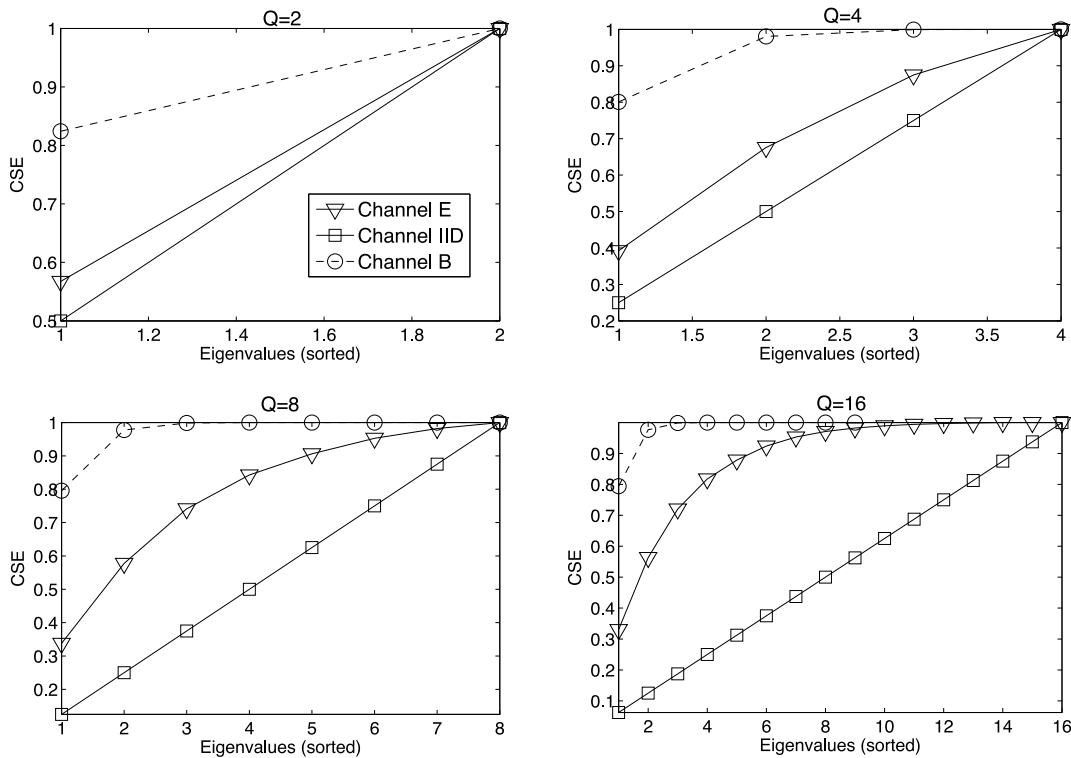


Fig. 3. Cumulative eigenvalue spread for Models B and E from (Erceg, 2003) and *iid* channel for different group sizes.

effect can be appreciated but to a much lesser extent, with the departure from the *iid* model being more evident for $Q = 16$ subcarriers. These results seem to indicate that, for Model B, $Q = 2$ would provide a good compromise between performance and detection complexity. In contrast, for channel E, $Q = 8$ would seem a more appropriate choice to fully exploit the channel characteristics. Notice that, according to the number of paths of each profile, Models B and E should attain diversity orders of 11 and 38, respectively. From the results in Fig. 3 it is obvious that far more moderate group sizes should be chosen in each case to operate in an optimal fashion from a diversity point of view at a reasonable (ML) detection complexity.

In conclusion, provided that scenarios with full spatial correlation are avoided, setting the number of subcarriers per group Q using the proposed CSE-based approach yields

$$\text{rank} \left(\mathbf{R}_g^{\min} \right) = Q N_T N_R. \tag{51}$$

On the rank of $\mathbf{G}_{g,c}^{\min}$: Given an $m \times n$ matrix \mathbf{A} and an $n \times p$ matrix \mathbf{B} , it holds that (Meyer, 2000)

$$\text{rank}(\mathbf{A}) + \text{rank}(\mathbf{B}) - n \leq \text{rank}(\mathbf{AB}) \leq \min \{ \text{rank}(\mathbf{A}), \text{rank}(\mathbf{B}) \}. \tag{52}$$

Thus, using optimally rotated spreading codes and setting the number of subcarriers per group Q using the proposed CSE-based approach, provided that pathological scenarios with full spatial correlation are avoided, we can use (46) and (51) in (52) to show that the global diversity order for the analysed MIMO strategies is given by

$$\tilde{D}_{\min} = \text{rank} \left(\mathbf{G}_{g,c}^{\min} \right) = \begin{cases} Q N_R & \text{SDM} \\ Q N_T N_R & \text{STBC/CDD.} \end{cases} \tag{53}$$

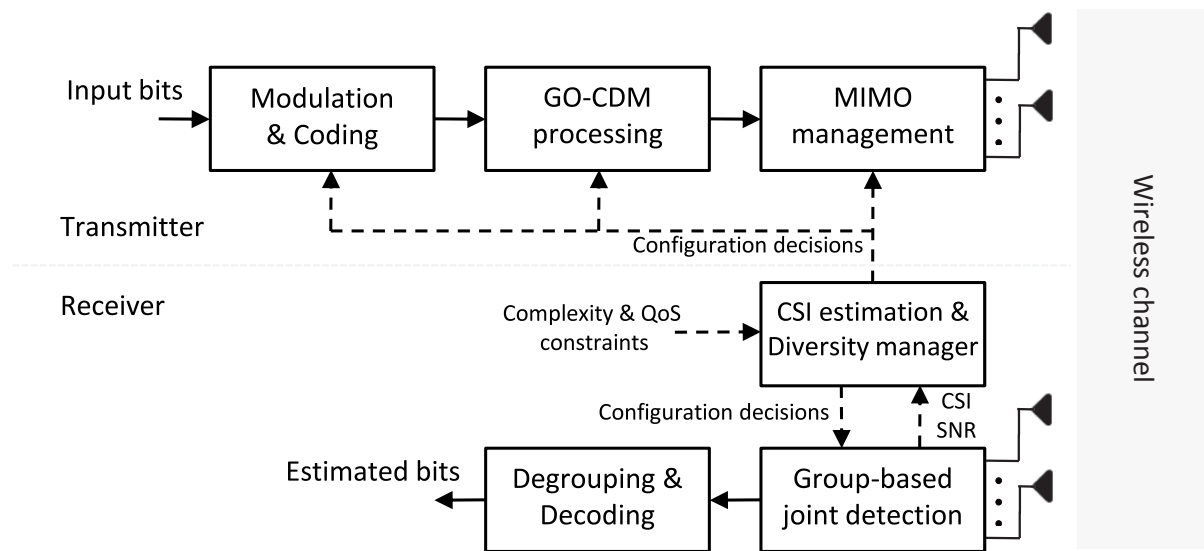


Fig. 4. Communication architecture for a MIMO-GO-CDM with group-size adaptation.

4. Reconfiguration strategies

It is clear from (44) and (53) that the (instantaneous) rank of the group frequency channel correlation matrix $\mathcal{R}_{h_g}^{\min}$ determines the asymptotic diversity of a MIMO-GO-CDM system, and therefore, it can form the basis for a group size adaptation mechanism. Strictly speaking, the maximum possible rank of $\mathcal{R}_{h_g}^{\min}$ is given by the number of independent paths in the channel profile. However, as shown in Subsection 3.3, very often the practical rank is far below this number as maximum diversity is only achieved at unrealistically low error rates. The adaptive group dimensioning scheme proposed next exploits this rank dependence to dynamically set the group size as a function of the channel response between all pairs of transmit and receive antennas. Figure 4 illustrates the architecture of the adaptive MIMO-GO-CDM system, where it can be appreciated that, in light of the acquired channel state information (CSI) and system constraints (complexity, QoS), the receiver determines the most appropriate group size to use and communicates this decision to the transmitter using a feedback channel. Note, as shown in Fig. 4, that CSI and SNR information can also be used to determine the most appropriate modulation and coding scheme in conjunction with the GO-CDM dimensioning and MIMO mode selection. However this topic is beyond the scope of this chapter and in this work only fixed modulation and uncoded transmission modes are considered.

In order to perform the adaptive dimensioning of the GO-CDM component, the receiver requires an estimate $\tilde{\mathcal{R}}_{h_g}^{\min}$ of the group frequency channel correlation matrix. An accurate estimate of the full correlation matrix $\mathcal{R}_{h_g}^{\min}$ could be computed by means of time averaging over the frequency domain, however, in indoor/WLANs scenarios where channels tend to vary very slowly, this approach would require of many OFDM symbols to get an adequate estimate. Fortunately, only the group channel correlation matrix is required, thus simplifying the correlation estimation. Exploiting the grouping structure of GO-CDM-MIMO-OFDM and assuming the channel frequency response is a wide-sense stationary (WSS) process, it is possible to derive an accurate estimate $\tilde{\mathcal{R}}_{h_g}^{\min}$ from the instantaneous CSI, provided the subcarriers in a given group have been chosen equispaced across the available bandwidth.

It is assumed that the group size to be determined is chosen from a finite set of possible values $\mathbf{Q} = \{Q^1, \dots, Q^{\max}\}$ whose maximum, Q^{\max} , is limited by the maximum detection complexity the receiver can support. Suppose that at block symbol k the receiver acquires knowledge of the channel to form the frequency response $\bar{\mathbf{h}}^{ij}(k)$ over all N_c subcarriers. Now, using the maximum group size available, Q^{\max} , it is possible to form the frequency responses for all $N_g^{\min} = N_c/Q^{\max}$ groups, $\{\bar{\mathbf{h}}_1^{ij}(k), \dots, \bar{\mathbf{h}}_{N_g^{\min}}^{ij}(k)\}$. Taking into account the WSS property it should hold that

$$E \left\{ \bar{\mathbf{h}}_{g,q}^{ij}(k) \bar{\mathbf{h}}_{g,v}^{ij}(k) \right\} = E \left\{ \bar{\mathbf{h}}_{m,q}^{i'j'}(k) \bar{\mathbf{h}}_{m,v}^{i'j'}(k) \right\}, \quad (54)$$

for all pairs of transmit and receive antennas (i, j) and (i', j') and any $q, v \in \{1, \dots, Q^{\max}\}$, as the correlation among any two subcarriers should only depend on their separation, not their absolute position or the transmit/receive antenna pair. A group channel correlation matrix estimate from a single frequency response can now be formed averaging across transmit and receive antennas, and groups,

$$\tilde{\mathbf{R}}_{h_g}^{\min} = \frac{1}{N_T N_R N_g^{\min}} \sum_{i=1}^{N_T} \sum_{j=1}^{N_R} \sum_{g=1}^{N_g^{\min}} \bar{\mathbf{h}}_g^{ij}(k) (\bar{\mathbf{h}}_g^{ij}(k))^H. \quad (55)$$

Using basic properties regarding the rank of a matrix, it is easy to prove that $\text{rank}(\tilde{\mathbf{R}}_{h_g}^{\min}) \leq \min(N_g^{\min}, Q^{\max})$, therefore, $N_g^{\min} = Q^{\max}$ maximises the range of possible group sizes using a single CSI shot. Let us denote the non-increasingly ordered positive eigenvalues of $\tilde{\mathbf{R}}_{h_g}^{\min}$ by $\tilde{\Lambda}_{h_g} = \{\tilde{\lambda}_{h_g,q}\}_{q=1}^{\tilde{Q}}$ where, owing to the deterministic character of $\tilde{\mathbf{R}}_{h_g}^{\min}$, they can all be assumed to be different and with order one, and consequently, \tilde{Q} represents the true rank of $\tilde{\mathbf{R}}_{h_g}^{\min}$. For the purpose of adaptation, and based on the CSE criterion, a more flexible definition of rank is given as

$$\tilde{Q}_\epsilon = \min \left\{ n : \Psi(n) = \frac{\sum_{q=1}^n \tilde{\lambda}_{h_g,q}}{\sum_{q=1}^{\tilde{Q}} \tilde{\lambda}_{h_g,q}} \geq 1 - \epsilon \right\}, \quad (56)$$

where $n \in \{1, \dots, \tilde{Q}\}$ and ϵ is a small non-negative value used to set a threshold on the normalised CSE. Notice that $\tilde{Q}_\epsilon \rightarrow \tilde{Q}$ as $\epsilon \rightarrow 0$.

Since the group size Q represents the dimensions of an orthonormal spreading matrix \mathbf{C} , restrictions apply on the range of values it can take. For instance, in the case of (rotated) Walsh-Hadamard matrices, Q is constrained to be a power of two. The mapping of \tilde{Q}_ϵ to an allowed group dimension, jointly with the setting of ϵ , permits the implementation of different reconfiguration strategies, e.g.,

$$\text{Maximise performance : } Q = \arg \min_{\hat{Q} \in \mathbf{Q}} \{\hat{Q} \geq \tilde{Q}_\epsilon\} \quad (57a)$$

$$\text{Minimise complexity : } Q = \arg \min_{\hat{Q} \in \mathbf{Q}} \{|\hat{Q} - \tilde{Q}_\epsilon|\}. \quad (57b)$$

It is difficult to assess the feedback involved in this adaptive diversity mechanism as it depends on the dynamics of the underlying channel. The suggested strategy to implement

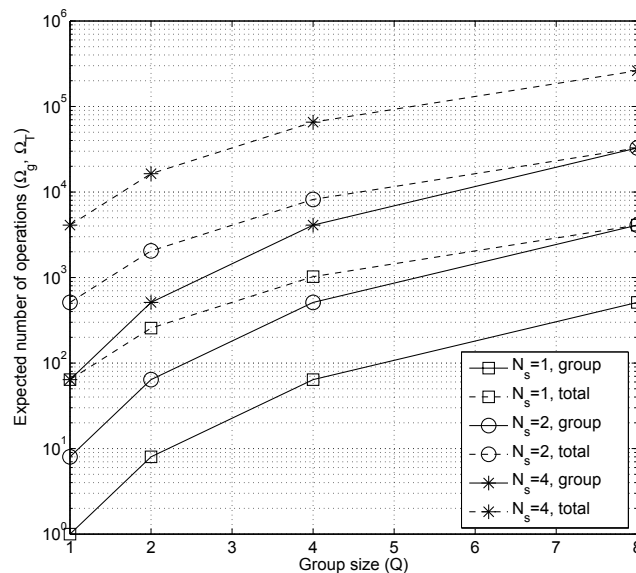


Fig. 5. Complexity as a function of group size (Q) for different number of transmitted streams.

this procedure is that the receiver regularly estimates the group channel rank and whenever a variation occurs, it determines and feeds back the new group dimension to the transmitter. In any case, the feedback information can be deemed insignificant as every update just requires of $\lceil \log_2 Q \rceil$ feedback bits with Q denoting the cardinality of set Q . Differential encoding of Q would bring this figure further down.

5. Computational complexity considerations

The main advantage of the group size adaptation technique introduced in the previous section is a reduction of computational complexity without any significant performance degradation. To gain some further insight, it is useful to consider the complexity of the detection process taking into account the group size in the GO-CDM component while assuming that an efficient ML implementation, such as the one introduced in (Fincke & Pohst, 1985), is in use. To this end, Vikalo & Hassibi (2005) demonstrated that the number of expected (complex) operations in an efficient ML detector operating at reasonable SNR levels is roughly cubic with the number of symbols jointly detected. That is, to detect one single group in a MIMO-GO-CDM system, $\Omega_g = \mathcal{O}(N_Q^3)$ operations are required.

Obviously, to detect all groups in the system, the expected number of required operations is given by $\Omega_T = \frac{N_c}{Q} \Omega_g$. Figure 5 depicts the expected per-group and total complexity for a system using $N_c = 64$ subcarriers, a set of possible group sizes given by $\{1, 2, 4, 8\}$ and different number of transmitted streams. Note that, in the context of this chapter, $N_s > 1$ necessarily implies the use of SDM. Importantly, increasing the group size from $Q = 1$ to $Q = 8$ implies an increase in the number of expected operations of more than two orders of magnitude, thus reinforcing the importance of rightly selecting the group size to avoid a huge waste in computational/power resources. Finally, it should be mentioned that for the STBC setup, efficient detection strategies exist that decouple the Alamouti decoding and GO-CDM

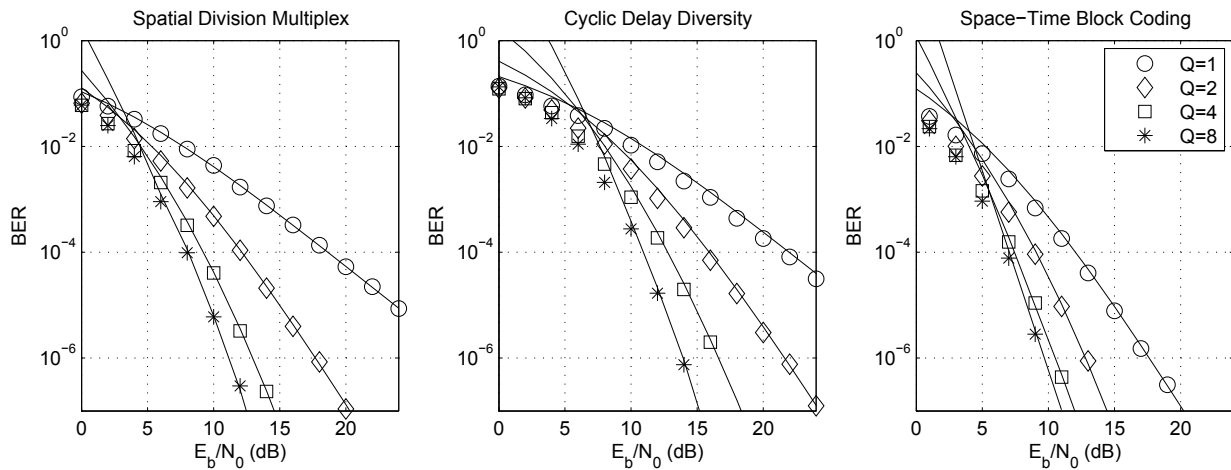


Fig. 6. Analytical (lines) and simulated (markers) BER for GO-CDM configured to operate in SDM (left), CDD (centre) and STBC (right) for different group sizes in Channel Profile E.

detection resulting in a simplified receiver architecture that is still optimum (Riera-Palou & Femenias, 2008).

6. Numerical results

In this section, numerical results are presented with the objective of validating the analytical derivations introduced in previous sections and also to highlight the benefits of the adaptive MIMO-GO-CDM architecture. The system considered employs $N_c = 64$ subcarriers within a $B = 20$ MHz bandwidth. These parameters are representative of modern WLAN systems such as IEEE 802.11n (IEEE, 2009). The GO-CDM technique has been applied by spreading the symbols forming a group with a rotated Walsh-Hadamard matrix of appropriate size. The set of considered group sizes is given by $Q = \{1, 2, 4, 8\}$. This set covers the whole range of practical diversity orders for WLAN scenarios while remaining computationally feasible at reception. Note that a system with $Q = 1$ effectively disables the GO-CDM component. For most of the results shown next, Channel Profile E from (Erceg, 2003) has been used. Perfect channel knowledge is assumed at the receiver. Regarding the MIMO aspects, the system is configured with two transmit and two receive antennas ($N_T = N_R = 2$). As in (van Zelst & Hammerschmidt, 2002), the correlation coefficient between Tx (Rx) antennas is defined by a single coefficient ρ_{Tx} (ρ_{Rx}). Note that in order to make a fair comparison among the different spatial configurations, different modulation alphabets are used. For SDM, two streams are transmitted using BPSK whereas for STBC and CDD, a single stream is sent using QPSK modulation, ensuring that the three configurations achieve the same spectral efficiency.

Figure 6 presents results for SDM, CDD and STBC when transmit and receive correlation are set to $\rho_{Tx} = 0.25$ and $\rho_{Rx} = 0.75$, respectively. The first point to highlight from the three subfigures is the excellent agreement between simulated and analytical results for the usually relevant range of BERs ($10^{-3} - 10^{-7}$). It can also be observed the various degrees of influence exerted by the GO-CDM component depending on the particular spatial processing mechanism in use. For example, at a $P_b = 10^{-4}$, it can be observed that in SDM and CDD, the maximum group size considered ($Q = 8$) brings along SNR reductions greater than 10 dB when compared to the setup without GO-CDM ($Q = 1$). In contrast, in combination with STBC, the maximum gain offered by GO-CDM is just above 5 dB. The overall superior performance of STBC can be explained by the fact that it exploits transmit and receive

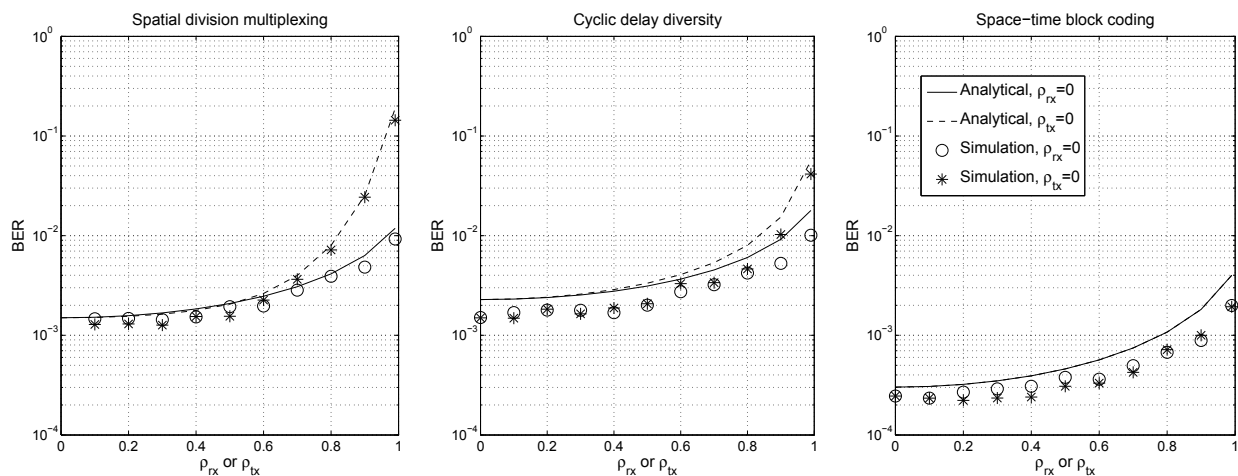


Fig. 7. Analytical (lines) and simulated (markers) BER for GO-CDM configured to operate in SDM (left), CDD (centre) and STBC (right) for different transmit/antenna correlation values.

diversity whereas in SDM there is no transmit diversity and in CDD, this is only exploited when combined with GO-CDM and/or channel coding.

Next, the effects of antenna correlation at either side of the communication link have been assessed for each of the MIMO processing schemes. To this end, the MIMO-GO-CDM system has been configured with $Q = 2$ and the SNR fixed to $E_s/N_0 = 10$ dB. The antenna correlation at one side was set to 0 when varying the antenna correlation at the other end between 0 and 0.99. As seen in Fig. 7, a good agreement between analytical and numerical results can be appreciated. The small discrepancy between theory and simulation is mainly due to the use of the union bound, which always overestimates the true error rate. In any case, the theoretical expressions are able to predict the performance degradation due to an increased antenna correlation. Note that, in CDD and SDM, for low to moderate values (0.0 – 0.7), correlation at either end results in a similar BER degradation, however, for large values (> 0.7), correlation at the transmitter is significantly more deleterious than at the receiver. For the STBC scenario, analysis and simulation demonstrate that it does not matter which communication end suffers from antenna correlation as it leads to exactly the same results. This is because all symbols are transmitted and received through all antennas (Tx and Rx) and therefore equally affected by the correlation at both ends.

Finally, the performance of the proposed group adaptive mechanism has been assessed by simulation. The SNR has been fixed to $E_s/N_0 = 12$ dB and a time varying channel profile has been generated. This profile is composed of *epochs* of 10,000 OFDM symbols each. Within an epoch, an independent channel realisation for each OFDM symbol is drawn (quasi-static block fading) from the same channel profile. For visualisation clarity, the generating channel profile is kept constant for three consecutive epochs and then it changes to a different one. All channel profiles (A-F) from IEEE 802.11n (Erceg, 2003) have been considered. Results shown correspond to an SDM configuration.

The left plot in Fig. 8 shows the BER evolution for fixed and adaptive group size systems as the environment switches among the different channel profiles. The upper-case letter on the top of each plot identifies the particular channel profile for a given *epoch*. Each marker represents the averaged BER of 10,000 OFDM symbols. Focusing on the fixed group configurations it is easy to observe that a large group size does not always bring along a reduction in BER. For example, for Profile A (frequency-flat channel) there is no benefit in pursuing extra frequency

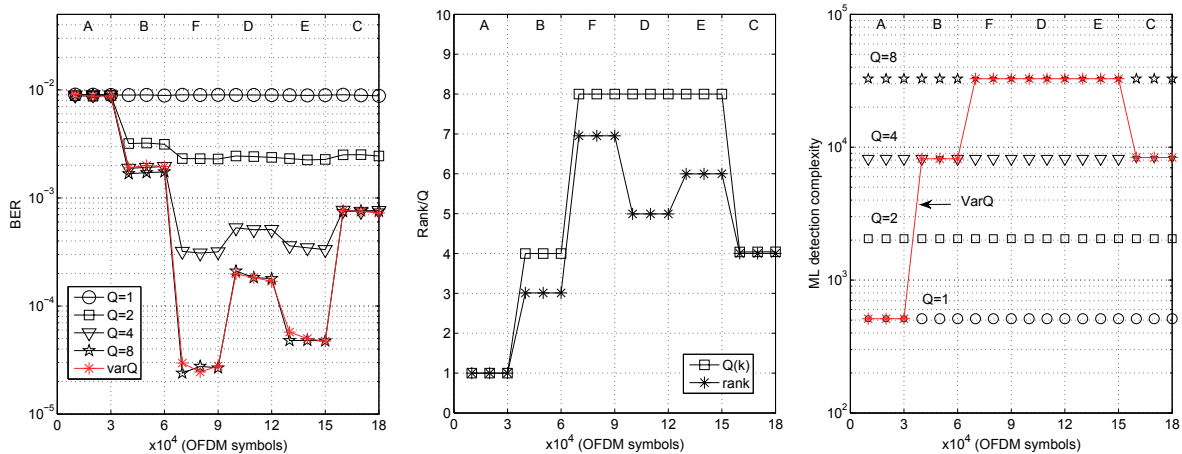


Fig. 8. Behaviour of fixed and adaptive MIMO GO-CDM-OFDM over varying channel profile using QPSK modulation at $E_s/N_0=12$ dB. $N_T = N_R = N_s = 2$ (SDM mode). Left: epoch-averaged BER performance. Middle: epoch-averaged rank/group size. Right: epoch-averaged detection complexity.

diversity at all. Similarly, for Profiles B and C there is no advantage in setting the group size to values larger than 4. This is in fact the motivation of the proposed MIMO adaptive group size algorithm denoted in the figure by *varQ*. It is clear from the middle plot in Fig. 8 that the proposed algorithm is able to adjust the group size taking into account the operating environment so that when the channel is not very frequency selective low Q values are used and, in contrast, when large frequency selectivity is sensed the group size dimension grows. Complementing the BER behaviour, it is important to consider the computational cost of the configurations under study. To this end the right plot in Fig. 8 shows the expected number of complex operations (see Section 5). In this plot it can be noticed the huge computational waste incurred, since there is no BER reduction, in the fixed group size systems with large Q when operating in channels with a modest amount of frequency-selectivity (A, B and C).

7. Conclusions

This chapter has introduced the combination of GO-CDM and multiple transmit antenna technology as a means to simultaneously exploit frequency, time and space diversity. In particular, the three most common MIMO mechanisms, namely, SDM, STBC and CDD, have been considered. An analytical framework to derive the BER performance of MIMO-GO-CDM has been presented that is general enough to incorporate transmit and receive antenna correlations as well as arbitrary channel power delay profiles. Asymptotic results have highlighted which are the important parameters that influence the practical diversity order the system can achieve when exploiting the three diversity dimensions. In particular, the channel correlation matrix and its effective rank, defined as the number of significant positive eigenvalues, have been shown to be the key elements on which to rely when dimensioning MIMO-GO-CDM systems. Based on this effective rank, a dynamic group size strategy has been introduced able to adjust the frequency diversity component (GO-CDM) in light of the sensed environment. This adaptive MIMO-GO-CDM has been shown to lead to important power/complexity reductions without compromising performance and it has the potential to incorporate other QoS requirements (delay, BER objective) that may result in further energy savings. Simulation results using IEEE 802.11n parameters have served to verify three

facts. Firstly, MIMO-GO-CDM is a versatile architecture to exploit the different degrees of freedom the environment has to offer. Secondly, the presented analytical framework is able to accurately model the BER behaviour of the various MIMO-GO-CDM configurations. Lastly, the adaptive group size strategy is able to recognize the operating environment and adapt the system appropriately.

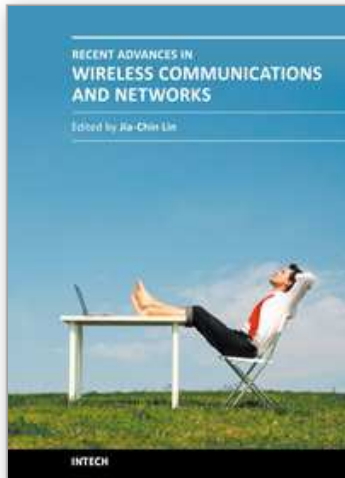
8. Acknowledgments

This work has been supported in part by MEC and FEDER under projects MARIMBA (TEC2005-00997/TCM) and COSMOS (TEC2008-02422), and a Ramón y Cajal fellowship (co-financed by the European Social Fund), and by Govern de les Illes Balears through project XISPES (PROGECIB-23A).

9. References

- Alamouti, A. (1998). A simple transmit diversity technique for wireless communications, *IEEE JSAC* 16: 1451–1458.
- Amari, S. & Misra, R. (1997). Closed-form expressions for distribution of sum of exponential random variables, *IEEE Trans. Reliability* 46(4): 519–522.
- Bauch, G. & Malik, J. (2006). Cyclic delay diversity with bit-interleaved coded modulation in orthogonal frequency division multiple access, *IEEE Trans. Wireless Commun.* 8: 2092–2100.
- Bury, A., Egle, J. & Lindner, J. (2003). Diversity comparison of spreading transforms for multicarrier spread spectrum transmission, *IEEE Trans. Commun.* 51(5): 774–781.
- Cai, X., Zhou, S. & Giannakis, G. (2004). Group-orthogonal multicarrier CDMA, *IEEE Trans. Commun.* 52(1): 90–99.
- Cimini Jr., L. (1985). Analysis and simulation of a digital mobile channel using orthogonal frequency division multiplexing, *IEEE Transactions on Communications* 33(7): 665–675.
- Craig, J. W. (1991). A new, simple and exact result for calculating the probability of error for two-dimensional signal constellations, *IEEE MILCOM'91 Conf. Rec.*, Boston, MA, pp. 25.5.1–25.5.5.
- Erceg, V. (2003). Indoor MIMO WLAN Channel Models. doc.: IEEE 802.11-03/871r0, Draft proposal.
- Femenias, G. (2004). BER performance of linear STBC from orthogonal designs over MIMO correlated Nakagami-m fading channels, *IEEE Trans. Veh. Technol.* 53(2): 307–317.
- Fincke, U. & Pohst, M. (1985). Improved methods for calculating vectors of short length in a lattice, including a complexity analysis, *Math. Comput.* 44: 463–471.
- Foschini, G. (1996). Layered space-time architecture for wireless communication in a fading environment when using multi-element antennas, *Bell Labs Technical Journal* 1(2): 41–59.
- Haykin, S. (2001). *Communication Systems*, 4th edn, Wiley.
- IEEE (2009). Part 11: Wireless LAN Medium Access Control (MAC) and Physical Layer (PHY) Specifications Amendment 5: Enhancements for Higher Throughput, *IEEE Std 802.11n-2009*.
- Johnson, R. & Wichern, D. (2002). *Applied Multivariate Statistical Analysis*, fifth edn, Prentice Hall.
- Kaiser, S. (2002). OFDM code-division multiplexing in fading channels, *IEEE Trans. Commun.* 50: 1266–1273.

- Meyer, C. (2000). *Matrix analysis and applied linear algebra*, Society for Industrial and Applied Mathematics (SIAM).
- Petersen, K. B. & Pedersen, M. S. (2008). The matrix cookbook. Version 20081110.
URL: <http://www2.imm.dtu.dk/pubdb/p.php?3274>
- Riera-Palou, F. & Femenias, G. (2008). Improving STBC performance in IEEE 802.11n using group-orthogonal frequency diversity, *Proc. IEEE Wireless Communications and Networking Conference*, Las Vegas (US), pp. 1–6.
- Riera-Palou, F. & Femenias, G. (2009). OFDM with adaptive frequency diversity, *IEEE Signal Processing Letters* 16(10): 837 – 840.
- Riera-Palou, F., Femenias, G. & Ramis, J. (2008). On the design of uplink and downlink group-orthogonal multicarrier wireless systems, *IEEE Trans. Commun.* 56(10): 1656–1665.
- Simon, M. & Alouini, M. (2005). *Digital communication over fading channels*, Wiley-IEEE Press.
- Simon, M., Hinedi, S. & Lindsey, W. (1995). *Digital communication techniques: signal design and detection*, Prentice Hall PTR.
- Stuber, G., Barry, J., McLaughlin, S., Li, Y., Ingram, M. & Pratt, T. (2004). Broadband MIMO-OFDM wireless communications, *Proceedings of the IEEE* 92(2): 271–294.
- Tarokh, V., Jafarkhani, H. & Calderbank, A. (1999). Space-time block codes from orthogonal designs, *IEEE Transactions on Information Theory* 45(5): 1456–1467.
- Telatar, E. (1999). Capacity of Multi-antenna Gaussian Channels, *European Transactions on Telecommunications* 10(6): 585–595.
- van Zelst, A. & Hammerschmidt, J. (2002). A single coefficient spatial correlation model for multiple-input multiple-output (mimo) radio channels, *Proc. Proc. URSI XXVIIth General Assembly*, Maastricht (the Netherlands), pp. 1–4.
- Vikalo, H. & Hassibi, B. (2005). On the sphere-decoding algorithm ii. generalizations, second-order statistics, and applications to communications, *Signal Processing, IEEE Transactions on* 53(8): 2819 – 2834.
- Weinstein, S. & Ebert, P. (1971). Data transmission by frequency-division multiplexing using the discrete Fourier transform, *IEEE Trans. Commun. Tech.* 19: 628–634.
- Wittneben, S. (1993). A new bandwidth efficient transmit antenna modulation diversity scheme for linear digital modulation, *Proc. IEEE Int. Conf. on Commun.*, Geneva (Switzerland), pp. 1630–1634.
- Yee, N., Linnartz, J.-P. & Fettweis, G. (1993). Multi-carrier CDMA in indoor wireless radio networks, *Proc. IEEE Int. Symp. on Pers., Indoor and Mob. Rad. Comm.*, Yokohama (Japan), pp. 109–113.



Recent Advances in Wireless Communications and Networks

Edited by Prof. Jia-Chin Lin

ISBN 978-953-307-274-6

Hard cover, 454 pages

Publisher InTech

Published online 23, August, 2011

Published in print edition August, 2011

This book focuses on the current hottest issues from the lowest layers to the upper layers of wireless communication networks and provides “real-time” research progress on these issues. The authors have made every effort to systematically organize the information on these topics to make it easily accessible to readers of any level. This book also maintains the balance between current research results and their theoretical support. In this book, a variety of novel techniques in wireless communications and networks are investigated. The authors attempt to present these topics in detail. Insightful and reader-friendly descriptions are presented to nourish readers of any level, from practicing and knowledgeable communication engineers to beginning or professional researchers. All interested readers can easily find noteworthy materials in much greater detail than in previous publications and in the references cited in these chapters.

How to reference

In order to correctly reference this scholarly work, feel free to copy and paste the following:

Felip Riera-Palou and Guillem Femenias (2011). Diversity Management in MIMO-OFDM Systems, Recent Advances in Wireless Communications and Networks, Prof. Jia-Chin Lin (Ed.), ISBN: 978-953-307-274-6, InTech, Available from: <http://www.intechopen.com/books/recent-advances-in-wireless-communications-and-networks/diversity-management-in-mimo-ofdm-systems>

INTECH
open science | open minds

InTech Europe

University Campus STeP Ri
Slavka Krautzeka 83/A
51000 Rijeka, Croatia
Phone: +385 (51) 770 447
Fax: +385 (51) 686 166
www.intechopen.com

InTech China

Unit 405, Office Block, Hotel Equatorial Shanghai
No.65, Yan An Road (West), Shanghai, 200040, China
中国上海市延安西路65号上海国际贵都大饭店办公楼405单元
Phone: +86-21-62489820
Fax: +86-21-62489821

© 2011 The Author(s). Licensee IntechOpen. This chapter is distributed under the terms of the [Creative Commons Attribution-NonCommercial-ShareAlike-3.0 License](#), which permits use, distribution and reproduction for non-commercial purposes, provided the original is properly cited and derivative works building on this content are distributed under the same license.

IntechOpen

IntechOpen